Available online at www.sciencedirect.com
SCIENCE DIRECT®
Chemical Physics Letters 381 (2003) 777–783
CHEMICAL PHYSICS LETTERS
www.elsevier.com/locate/cplett

Extensive, high-resolution measurement of hyperfine interactions: precise investigations of molecular potentials and wave functions

Lisheng Chen, Jun Ye *

JILA, National Institute of Standards and Technology and University of Colorado, Boulder, CO 80309-0440, USA

Received 29 August 2003; in final form 15 October 2003
Published online: 4 November 2003

Abstract

We report high-resolution and high-precision measurement of hyperfine interactions of the first excited electronic state (B) of I_2 over an extensive range of vibrational and rotational quantum numbers. Systematic variations in the hyperfine parameters, including both rovibrational level dependence and internuclear separation dependence, are confirmed by calculations based on ab initio molecular potential energy curves and electronic wave functions derived from a separated-atom basis set. We have accurately determined the state-dependent quantitative changes of hyperfine interactions caused by perturbations from other electronic states and identified the respective perturbing states.
© 2003 Published by Elsevier B.V.

1. Introduction

The hyperfine structure of rovibrational levels originates from additional nucleus–electron and nucleus–nucleus interactions that are not included in the molecular Hamiltonian under the Born–Oppenheimer framework. The advent of laser saturation spectroscopy enabled early pioneering work to identify four contributions to the I_2 hyperfine Hamiltonian: nuclear electric quadrupole (eqQ) [1], spin–rotation (C) [2,3], tensorial spin–spin (d) [4], and scalar spin–spin (δ) [5,6] interactions. Agreement between experiment and theory using the four-term hyperfine Hamiltonian is at the kilohertz level for a few selected transitions. It is agreed that the existence of δ in the first excited electronic state B is due solely to perturbations from higher electronic states [5] and that the rapid increase of C with ascending vibrational quantum number v' is due to perturbations from two 1_u states sharing the same $^2P_{3/2} + {}^2P_{1/2}$ dissociation limit with B. Calculations have been carried out for only a few isolated rovibrational levels scattered from $v' = 40$ to 82 [7–11], and they agree with the global trend of vibrational dependence, but lack detailed information about the rotational dependence. For vibrational levels of B below $v' = 43$, functional forms on the state-dependent variations of the hyperfine interactions have been investigated intensively from empirical data, but

* Corresponding author. Fax: +1-303-492-5235.
E-mail address: Ye@jila.colorado.edu (J. Ye).

0009-2614/$ - see front matter © 2003 Published by Elsevier B.V.
doi:10.1016/j.cplett.2003.10.052

more work is needed to construct physical models of the corresponding molecular structure [12].

Combining absolute optical frequency metrology with high-resolution and broad wavelength-coverage laser spectroscopy, we present in this Letter a systematic high-precision investigation of hyperfine interactions associated with I_2 transitions in the wavelength region of 530–500 nm. This is an important region for the study of I_2 molecular structure since the associated vibrational levels (around $v' = 42$ up to 70) of B stretch from a closely bonded molecular basis to a separated-atom basis appropriate for the $^2P_{3/2} + {}^2P_{1/2}$ dissociation limit. Studies of a large set of rovibrational quantum numbers provide systematic information on state-dependent variations in the hyperfine interactions caused by perturbations from other nearby states. The narrow-linewidth I_2 transitions in this wavelength region also provide excellent cell-based optical frequency references for laser stabilization. Our work is made possible by two recent key experimental advances. The first is the generation of highly stable and widely tunable light sources in this wavelength region using a frequency doubled CW Ti:sapphire laser whose wavelength coverage extends from the traditional 800 nm to beyond 1.06 μm [13]. The second is the capability for absolute optical frequency measurement empowered by a femtosecond laser-based optical frequency comb [14]. These capabilities have allowed precision molecular spectroscopy to be carried out systematically across a vast spectral window, providing kHz-level line accuracies for most hyperfine components on 79 rovibrational transitions in the targeted wavelength range. Careful analysis leads to accurate determination of the molecular structure over a large dynamic range, fully delivering the potential of frequency metrology based laser spectroscopy where a detailed and yet global picture of molecular structure can be efficiently constructed.

With selected rovibrational transitions studied and their associated four-term hyperfine interactions determined within the spectral window of 530–500 nm, we have investigated in theory the hyperfine Hamiltonian using ab initio molecular potential energy curves constructed from a separated-atom basis set and the associated electronic wave functions. We have extended the range of separated-atom basis calculations from levels near the dissociation limit to low vibrational levels ($v' = 5$) and have found very good agreement with the experimental data on both vibrational and rotational dependences. It is worth emphasizing that our investigation provides the first (ab initio) theoretical understanding of the rotational dependence that is confirmed by our experimental data. As an example, we will present an explicit calculation on C_B (for the B state). We have also for the first time explored the abnormal variations of eqQ_B, d_B, and δ_B caused by strong perturbations in the vicinity of $57 \leqslant v' \leqslant 59$, which deviate from the usual monotonic trend observed for other vibrational levels. Furthermore, we have transformed rovibrational quantum numbers into corresponding internuclear separations, providing a semi-classical view of how hyperfine interactions vary with physical internuclear separations. Overall, the work reported in this Letter reveals a clear physical picture connecting the separated-atom model and the tightly bounded molecule model.

2. Experiment

A widely tunable and frequency-stabilized laser source is used to probe saturated-absorption resonances of I_2 using a frequency modulation technique. The laser is pre-stabilized by a stable optical cavity and its absolute optical frequency is calibrated by a femtosecond laser comb linked to the primary Cs standard. Most of the hyperfine-splitting measurements are carried out by the cavity-based laser frequency scan, which is enabled by a double-passed acousto-optic modulator located in front of the fixed-length cavity. Some of the hyperfine components have their absolute frequencies measured by the comb. The effective hyperfine parameters of the B state are determined by fitting the hyperfine splitting patterns of the B–X transition to a four-term effective hyperfine Hamiltonian [7] with residual fit errors ~10 kHz. To ensure a reliable separation of the B state parameters from the X state's, we select the transitions originating from only the vibrational ground state ($v'' = 0$)

and fix the J-dependence of the ground level hyperfine parameters to that predetermined by interpolation formula [12,15]. More detailed experimental information and extensive data record on the B state hyperfine parameters will be provided in a forthcoming publication [16].

3. Results and discussions

3.1. Rovibrational dependence and strong perturbation in the region of $42 \leqslant v' \leqslant 70$

All four hyperfine parameters exhibit systematic rovibrational dependence in the measured vibrational levels of B from $v' = 42$ to 70. Fig. 1 illustrates respective variations for each parameter. Each solid line is a fit of the experimental data for rotational dependence belonging to a single vibrational level (v' indicated in the figure). In general, all hyperfine parameters have monotonic dependence on both rotational and vibrational quantum numbers except for the levels in the vicinity of $v' = 57$–59. However, the v-dependence of eqQ_B reverses its trend after $v' = 60$ and hence their values for higher v' levels overlap those of lower v' levels. For the sake of figure clarity, the eqQ_B measurement data for $v' > 60$ are not shown.

Another important observation is that for the levels of $v' = 57$ and 59 all hyperfine parameters except for C_B bear abnormal J-dependences that resemble one another. The abnormality implies a strong perturbation from some nearby electronic states, leading to the rather large residual errors (50–100 kHz) in the associated hyperfine fits. The perturbation's origin can be traced back to a $1_g(^1\Pi_g)$ state located inside a cluster of electronic states sharing the same dissociation limit with the B state. Among this group of states, the $1_g(^1\Pi_g)$ state has a potential energy curve (PEC) whose outer limb is closest to that of the B state. This suggests that as the two sets of the rovibrational

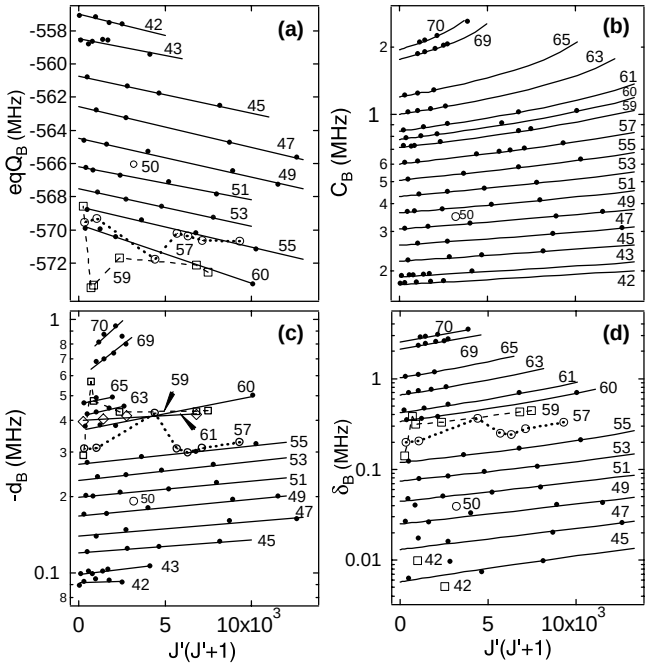

Fig. 1. Rovibrational dependence of the B state hyperfine parameters: (a) eqQ_B, (b) C_B, (c) d_B, and (d) δ_B. Note (b), (c), and (d) are semilog plots and the vertical scale of (c) has been inverted. Each solid line is a fit for J-dependence for each vibrational level (v' indicated in the figure). Experimental data in squares and open circles show abnormal variations of eqQ_B, d_B, and δ_B around $v' = 57$ and 59.

levels progress within the B and $1_g(^1\Pi_g)$ states, energy coincidences and relatively large Franck–Condon overlaps (~0.1 in magnitude) between the B and $1_g(^1\Pi_g)$ rovibrational levels can arise simultaneously. This would induce strong hyperfine perturbation that dramatically alters hyperfine spectra and imposes irregularities on smoothly varying hyperfine parameters arising from weak perturbations. Owing to the relatively large differences in the vibrational and rotational constants for the $1_g(^1\Pi_g)$ and B states over the vibrational levels of interest, these resonances each spans only a small range of rotational levels, a feature which is clearly identified in Fig. 1. These abnormal variations directly confirm the previously observed u–g mixing between the $1_g(^1\Pi_g)$ and B states at rotational levels centered on $J' = 22$ at $v' = 59$ through the optical–optical double-resonance experiment in which the high-lying ion-pair states with u symmetry were accessed [17].

3.2. Vibrational dependence in the B state

Combining data from this work and the literature (see [11,12], and references therein), investigations of the hyperfine spectra now cover the majority of the vibrational levels in the B state. Therefore, it is now possible and useful to explore the global trend of these hyperfine parameters in the B state. Suppressing the rotational dependence, hyperfine parameters as functions of pure vibrational energy $E(v')$ are illustrated in Fig. 2. As shown in the figure, the values of these hyperfine parameters increase rapidly when molecules approach the dissociation limit, which is a result of the increasingly strong perturbations from other high-lying electronic states sharing the same dissociation limit with B. While C_B's variation is smooth over the whole range, eqQ_B, d_B, and δ_B all have local irregularities at three positions: $v' = 5$, where the $B''1_u(^1\Pi_u)$ state crosses nearby [18], around $v' = 57$–59 (see discussions above), and from $v' = 76$ to 78 ,where a strong perturbation is present due to $1_g(^1\Pi_g)$ state [11].

3.3. R-dependence of the hyperfine interaction

To examine these hyperfine parameters in terms of internuclear separation R, the vibrational average of the hyperfine parameters is removed by inverting the expression $O(v', J') = \langle v'_{J'}|O(R)|v'_{J'}\rangle$ [19,20], where $O(v', J')$ denotes one of the four hyperfine parameters. The inversion is done by expanding the function $O(R)$ as a polynomial with its coefficients determined from experimental fit. Fig. 3 plots eqQ_B, C_B, d_B, and δ_B against R-centroid evaluated from $\langle v'_{J'}|R|v'_{J'}\rangle$ ($|v'_{J'}\rangle$ properly normalized), along with the corresponding residual errors of the interpolation. In Fig. 3a–d, solid lines are calculated from $\langle v'_{J'}|O(R)|v'_{J'}\rangle$ and symbols are experimental data. In consistence with C_B's smooth variation, the interpolation function

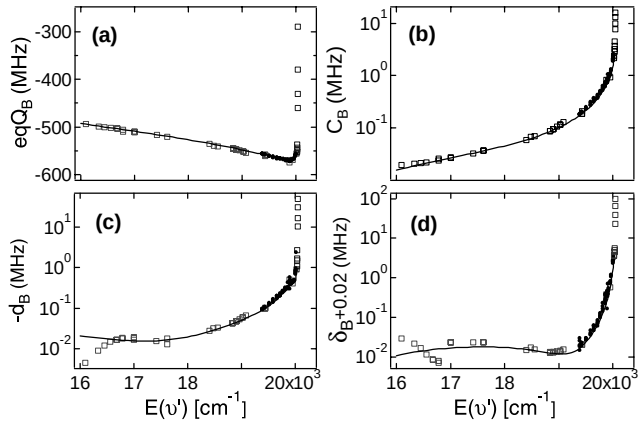

Fig. 2. Vibrational dependence of the B state hyperfine parameters: (a) eqQ_B, (b) C_B, (c) d_B, and (d) δ_B. Symbols are experimental data (dots: this work, squares: literature). Solid lines are fits for the experimental data.

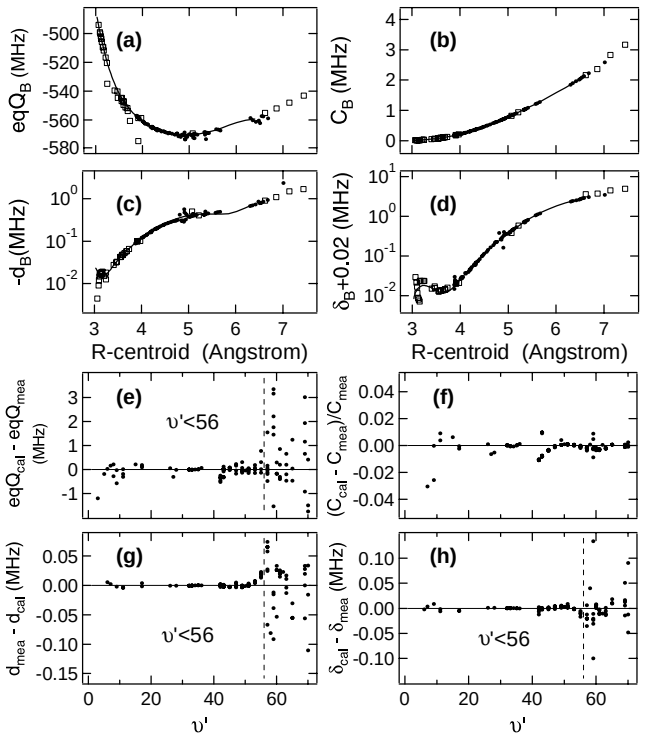

Fig. 3. (a) eqQ_B, (b) C_B, (c) d_B, and (d) δ_B versus R-centroid. Solid lines are calculated from $\langle v'_{J'}|O(R)|v'_{J''}\rangle$. Symbols are experimental data (dots: this work, squares: literature). (e)–(h) show residual errors of the interpolation. See text for details.

$C_B(R)$ has small residual errors (within ± 0.03, relative) for the entire range from $v' = 3$ to 70 as shown in Fig. 3f. In contrast, the large residual errors in the interpolation of eqQ_B, d_B, and δ_B for $v' \geqslant 56$ reflect their abnormal variations observed around $v' = 57$ and 59, restricting a reliable interpolation only to levels of $v' < 56$.

In the region of $R < 5$ Å, valuable information can be readily extracted from eqQ_B to assist the investigation of I_2's electronic structure. Unlike the other three hyperfine parameters whose major parts originate from perturbations at nearly all possible values of R, a significant part of eqQ_B is due to the interaction between the nuclear quadrupole moment Q and the local electric field gradient $q(R)$ generated by the surrounding charge distribution of a largely B state character. This fact is more evident if we focus on the region of $R < 5$ Å, where perturbations from other electronic states are negligible by comparison. In addition, for $R < 5$ Å, eqQ_B deviates gradually from what is predicated by the separated-atom basis model or linear combinations of atomic orbital model [21]. Thus, for $R < 5$ Å, the vibration-removed interpolation function $eqQ_B(R)$, coupled with a priori information on $q(R)$, can be used to determine iodine nuclear quadrupole moment or serve as a benchmark for molecular ab initio calculations of the electronic structure at various values of R.

3.4. Ab initio calculations

In addition to metrological applications, these precision measurements on B–X hyperfine spectra provide an alternative and yet effective way to investigate the PECs and electronic wave functions of these states that converge with the B state. To demonstrate this, we perform a calculation of C_B based on the available PECs and the electronic wave functions derived from a separated-atom basis set. The dominant part of C_B is due to perturbations from two 1_u states coupled by the

gyroscopic Hamiltonian (off-diagonal part of the rotational Hamiltonian) and the magnetic dipole interactions between the nuclei and the surrounding electrons [7]. Up to the second-order perturbation, C_B can be written as [7–11]

$$C_B = -2\sum_{\Omega'}\left[\sum_{v'}\frac{\langle V^0\rangle\langle V^1(a)\rangle}{E_{0_u^+vJ}-E_{\Omega'v'J}} + \int\frac{\langle V^0\rangle\langle V^1(a)\rangle}{E_{0_u^+vJ}-E_{\Omega'J}}\rho(E_{\Omega'J})\,\mathrm{d}E_{\Omega'J}\right], \quad (1)$$

where $E_{0_u^+vJ}$ and $E_{\Omega'v'J}$ are the energies of discrete rovibrational levels located, respectively, in the B and the perturbing states, and $E_{\Omega'J}$ and $\rho(E_{\Omega'J})$ are energy and the corresponding density of states in the energy continuum above the potential asymptote. $\langle V^0\rangle\sqrt{2J(J+1)}$ is the off-diagonal matrix element of the gyroscopic Hamiltonian and $\langle V^1(a)\rangle$ is the reduced matrix element of the spherical tensor operator describing the magnetic dipole interactions for nucleus a in the molecular frame. We approximate each matrix element as a product of a Franck–Condon integral and a matrix element that involves only electronic wave functions. Because molecular electronic wave functions of practical use are not available, we instead use the wave functions derived from a separated-atom basis set [8] and relate the reduced electronic matrix elements to atomic hyperfine parameters. For the two 1_u states, we use ab initio PECs [22] (empirically improved by the ground state PEC) for $R \leqslant 6.35$ Å and long-range PECs [23] for $R \geqslant 7$ Å, respectively, with the former shifted vertically by a small amount to match the corresponding long-range one. The combined 1_u PECs, together with the B state empirical potential [24], allow the construction of the radial wave functions and hence the computation of Franck–Condon integrals for discrete levels and energy continua [25,26]. Once these PECs are chosen, the only adjustable parameter in the calculation is the admixture of the electronic wave functions of the two 1_u states.

We calculate the vibrational dependence of C_B for $v' = 5$–73 (R-centroid from 3 to 7.8 Å) with J' fixed to 1 (dotted line in Fig. 4a), as well as the J-dependence of C_B at two vibrational levels of $v' = 70$ and 47 (dotted lines in Fig. 4b and c). For both vibrational and rotational dependences, the ab initio results agree very well with the experimental data for $v' \geqslant 42$ (R-centroid $\geqslant 3.9$ Å). For $v' \leqslant 42$, theory calculations start to deviate slightly from the experimental data. This discrepancy at small internuclear separations is mainly correlated with the fact that in our calculation the admixture

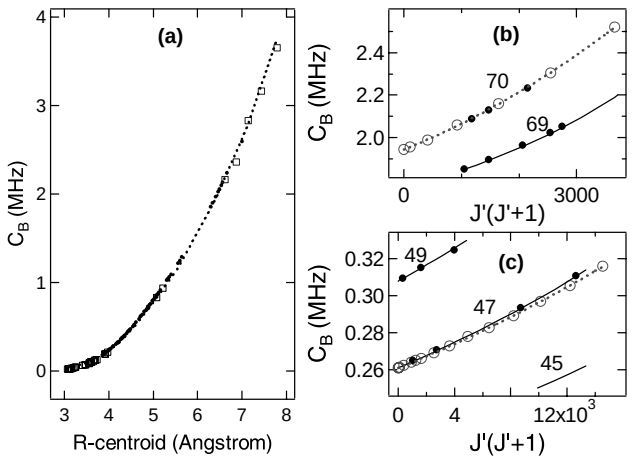

Fig. 4. Theoretical calculation of C_B. (a) R-centroid dependence for $5 \leqslant v' \leqslant 75$ with J' fixed to 1 and J-dependence for (b) $v' = 70$ and (c) $v' = 47$. The dotted and solid lines are the fits to the calculated results (empty circles) and experimental data (dots: this work, squares: literature), respectively.

of the electronic wave functions of the two 1_u states is held fixed for all values of R involved. It may be possible to improve the calculation at small R using recently obtained molecular wave functions [27]. Another interesting fact is that for high rovibrational levels, the energy continua in the perturbing states contribute significantly to C_B through the Franck–Condon overlap. This suggests an approach to recover the experimental information on the repulsive part of the PECs of these perturbing electronic states which is otherwise inaccessible by a direct photodissociation excitation from the ground electronic state X due to small Franck–Condon overlaps. Finally, it is clear that eqQ_B, d_B, and δ_B can also be treated in the same manner. However, more perturbing states are involved due to different types of coupling terms [7]. The detailed calculations for these hyperfine parameters will be published elsewhere.

4. Conclusion

In summary, the optical-frequency-based systematic mapping of the hyperfine interactions ranging from $v' = 42$ to 70 in the I_2 B state has yielded rich information about the rovibrational dependence of the hyperfine parameters. We have gained valuable knowledge about molecular structure such as molecular potential curves, electronic wave functions, and perturbations from nearby states. Models such as the separated-atom basis set can now be carefully checked by comparing experimental hyperfine data against calculations using molecular PECs.

Acknowledgements

We acknowledge important contributions made by W.-Y. Cheng and J.L. Hall to this work. We thank W.A. de Jong for sharing his numerical results on the I_2 potential energy curves. This research is supported by NASA, NSF, ONR, and NIST.

References

[1] M. Kroll, K.K. Innes, J. Mol. Spectrosc. 36 (1970) 295.
[2] G.R. Hanes, C.E. Dahlstrom, Appl. Phys. Lett. 14 (1969) 362.
[3] T.W. Hänsch, M.D. Levenson, A.L. Schawlow, Phys. Rev. Lett. 26 (1971) 946.
[4] P.R. Bunker, G.R. Hanes, Chem. Phys. Lett. 28 (1974) 377.
[5] N.F. Ramsey, E.M. Purcell, Phys. Rev. 85 (1952) 143L.
[6] B.M. Landsberg, Chem. Phys. Lett. 43 (1976) 102.
[7] M. Broyer, J. Vigué, J.C. Lehmann, J. Phys. (Paris) 39 (1978) 591.
[8] J. Vigué, M. Broyer, J.C. Lehmann, Phys. Rev. Lett. 42 (1979) 883.
[9] J.P. Pique, F. Hartmann, R. Bacis, S. Churassy, Opt. Commun. 36 (1981) 354.
[10] J.P. Pique, R. Bacis, M. Broyer, S. Churassy, J.B. Koffend, J. Chem. Phys. 80 (1984) 1390.
[11] J.P. Pique, F. Hartmann, S. Churassy, R. Bacis, J. Phys. (Paris) 47 (1986) 1917.
[12] B. Bodermann, H. Knöckel, E. Tiemann, Eur. Phys. J. D 19 (2002) 31.
[13] W.Y. Cheng, L.S. Chen, T.H. Yoon, J.L. Hall, J. Ye, Opt. Lett. 27 (2002) 1076.
[14] T. Udem, J. Reichert, R. Holzwarth, T.W. Hänsch, Phys. Rev. Lett. 82 (1999) 3568.
[15] F.-L. Hong, J. Ye, L.-S. Ma, S. Picard, C.J. Bordé, J.L. Hall, J. Opt. Soc. Am. B 18 (2001) 379.
[16] L. Chen, W.-Y. Cheng, J. Ye, J. Opt. Soc. Am. B (submitted).
[17] P.J. Jewsbury, T. Ridley, K.P. Lawley, R.J. Donovan, J. Mol. Spectrosc. 157 (1993) 33.
[18] J. Vigué, M. Broyer, J.C. Lehmann, J. Phys. (Paris) 42 (1981) 949.
[19] V. Špirko, J. Blabla, J. Mol. Spectrosc. 129 (1988) 59.
[20] W.S. Barney, C.M. Western, K.C. Janda, J. Chem. Phys. 113 (2000) 7211.
[21] R. Bacis, M. Broyer, S. Churassy, J. Vergès, J. Vigué, J. Chem. Phys. 73 (1980) 2641.
[22] W.A. de Jong, L. Visscher, W.C. Nieuwpoort, J. Chem. Phys. 107 (1997) 9046.
[23] M. Saute, M. Aubert-Frécon, J. Chem. Phys. 77 (1982) 5639.
[24] S. Gerstenkorn, P. Luc, C. Amiot, J. Phys. (Paris) 46 (1985) 355.
[25] R.J. Le Roy, University of Waterloo, Report No. CP-655, 2002.
[26] R.J. Le Roy, G.T. Kraemer, University of Waterloo, Report No. CP-650R, 2002.
[27] E.A. Pazyuk, A.V. Stolyarov, V.I. Pupyshev, N.F. Stepanov, S.Y. Umanskii, A.A. Buchachenko, Mol. Phys. 99 (2001) 91.